J. Comp. Appl. Res. Mech. Eng. Vol. 12. No. 2, pp. 177-191, 2023 *DOI: 10.22061/JCARME.2022.6916.1894*

Journal of Computational and Applied Research in Mechanical Engineering
jcarme.sru.ac.ir
SRTTU
JCARME
ISSN: 2228-7922

Research paper

Numerical response using finite strip element including drilling degree of freedom

J. Akbari[a,*], H. Valaei[a] and M. F. Sepahvand[b]

[a] *Department of Civil Engineering, Bu-Ali Sina University, Hamedan, Iran*
[b] *Department of Civil Engineering, Faculty of Engineering, Khorramabad Branch, Islamic Azad University, Khorramabad, Iran*

Article info:

Article history:

Received: 22/05/2020
Revised: 18/05/2022
Accepted: 20/05/2022
Online: 23/05/2022

Keywords:
Finite strip element,
FSE,
Finite element method,
Rotational DOF,
Drilling,
Numerical response.

[*]Corresponding author:
j.akbari@basu.ac.ir &
jalal.akbari@gmail.com

Abstract

Finite-element modeling of structures using elements without rotational degrees of freedom (DOFs) is usually stiffer than their physical behavior. Therefore, the stiffness of a structural system will be smoothed by adding rotational DOFs in the numerical model. In the traditional displacement-based finite-element method, adding drilling rotations is not easy. The main contribution of this paper is performing dynamic analyses using the finite strip element with added drilling rotations to the elements. For this purpose, any quadrilateral area is divided into two independent sets of orthogonal strips comprising truss and Bernoulli-Euler beam elements. Then, by using new shape functions, mass, damping, stiffness matrices, and equivalent nodal forces are derived. Finally, time history analysis for plane stress or strain type problems for direct earthquake records is performed using the developed formulations. The numerical studies show that the results of the finite strip method using coarse meshes are competitive with the results of the finite-element method using fine meshes. This advantage is valuable in time-consuming computational problems, e.g., dynamic or nonlinear analyses.

1. Introduction

To calculate the numerical responses of any structure using the finite-element method, the domain of the problem is usually discretized into three-dimensional (3D) elements. However, analyzing problems using 3D elements is a time-consuming process, and in the case of nonlinear or dynamic analyses, the process is not cost-efficient. Nevertheless, many problems in civil and mechanical engineering fields could be simplified as a 2D model, and using triangular or rectangular elements is more common. The main disadvantage of three-node triangular elements is that they are constant strain triangular (CST) elements and cannot simulate the variations of the stress field over the domain of the element. Accordingly, for appropriate evaluation of

stresses, fine meshes of CST elements should be created. Therefore, instead of using CST elements, rectangular or quadrilateral elements are used. Standard four-node rectangular elements usually comprise eight-translational degrees of freedom (DOFs) or sixteen DOFs (eight-translational and eight-rotational DOFs). Generally, the finite-element modeling of structures by elements without rotational DOFs is stiffer than the real behavior of the structures. Accordingly, adding rotations in the nodes of the elements will smooth the stiffness matrix. In the traditional displacement-based finite-element method, adding drilling rotations in the elements is difficult.

Four-node rectangular elements that include sixteen DOFs, eight-translational and eight-rotational DOFs are used for solving plate-bending type problems and are not useful for plane stress or strain type ones. The formulation of these kinds of elements, including four DOFs in each node, is complicated, and the dimensions of mass and stiffness matrices are 16×16; and therefore, in comparison with four-node solid elements, are not cost-effective. Consequently, it is interesting to define a planar solid element with a drilling rotational degree of freedom at nodes, which can improve the performance and accuracy of numerical simulations.

For the finite strip element (FSE) method, Wang R.H presented a theory to construct membrane elements with a rotational degree of freedom; and the method is named a finite belt method [1]. Huang & Thambiratnam applied the FSE method for analyzing plates resting on elastic foundations [2]. Liu, G.R used the combined FSE and finite-element method for analyzing the scattering of elastic waves in laminates [3]. Liu *et al*. applied the strip element method for shape discrimination of strip rolling [4]. Xia *et al.* proposed the membrane element with rotational degrees of freedom for beam-type structures for static analyses [5]. Rojas *et al.* used a quadrilateral layered membrane element with drilling degrees of freedom for nonlinear static modeling of reinforced concrete walls [6]. Also, Wang and Jiang used this method for static analysis of curved box girder cells [7].

The FSE method for buckling analysis of thin-walled members has been applied by many researchers, e.g.: Schafer [8], Schafer and Adnay [9], Eccher *et al*. [10], Ghannadpour *et al*. [11], Yao *et al.* [12], Chen and Qiao) [13], He *et al.* [14]. Similalry, in the area of steel member design, Li and Schafer [15], Zhen *et al.* [16], and Ajeesh and Jayachandran [17] have applied the FSE element in various steel components design problems. Chen and Qiao utilized the FSE method [18] for post-buckling analysis of plates under shear and compression loadings,. In vibration and dynamic analysis fields, several types of research can be mentioned, e.g., Wang and Zhang [19], Jiang and Au [20], Poblet and Rodriguezz [21], and Senjanovic *et al.* [22].

In the above-mentioned literature, several studies have been performed using the FSE element method under static loading only; however, for time-dependent loadings, no direct formulations, including drilling DOF, could be found. The authors believe that the characteristics of time-dependent problems are not similar to static ones. The stiffness, damping, and mass parameters of the structures are usually affected by the structural responses during the dynamic excitations. Moreover, for static cases, the system responses are influenced only by the stiffness of any system. Here, to develop the FSE formulation, a rectangular element is divided into two independent sets of orthogonal strips using truss and Bernoulli beam type elements. Then, mass, damping, stiffness matrices, and the equivalent nodal forces are obtained based on the proposed shape functions. Subsequently, dynamic analyses of plane stress/strain type problems against earthquake records are performed. Without losing the generality of the proposed formulation, this method could be used for any domain and it is not limited to a rectangular area. For non-rectangular areas, simple mapping techniques should be used to convert the skew domains into rectangular or square.

All steps of the presented formulations are programmed in a MATLAB environment [23]. The numerical studies reveal that the results of the FSE method using coarse meshes are competitive with the results of the finite-element method using fine meshes. This advantage is important in time-consuming computational cases such as dynamic or nonlinear analyses.

2. Formulation of FSE method

According to Fig. 1, consider a rectangular element with three degrees of freedom at each node, and twelve DOFs in each element. Here, u_i, v_i are the translational degrees of freedoms, and θ_i is the drilling rotations.
As seen from Fig. 2, to obtain the shape functions, extracting the stiffness and mass matrices, and force vectors, the rectangular area is divided into two orthogonal truss and beam elements. Therefore, each node has three degrees of freedom, and the quantities at any point are calculated by $u_L\ u_R\ v_B\ v_U$ interpolation parameters. The vales of these shape functions and strain-displacement matrix of the FSE are calculated in Section 2.1.

2.1. Shape function and strain matrix

In the finite-strip elements, FSE, a linear polynomial function for axial displacements, and cubic polynomial for transverse displacements are used, and the displacement functions are written as Eq. (1):

$$\begin{aligned} u &= [M_1 \quad M_2]\{u_L \quad u_R\}^T \\ v &= [\bar{M}_1 \quad \bar{M}_2]\{v_B \quad v_U\}^T \end{aligned} \tag{1}$$

in which $M_1, M_2, \bar{M}_1, \bar{M}_2$ are linear interpolation functions, and are written as Eq. (2).

$$\begin{aligned} M_1 &= (1-r)/2 \quad M_2 = (1+r)/2 \quad r = x/a \\ \bar{M}_1 &= (1-s)/2 \quad \bar{M}_2 = (1+s)/2 \quad s = y/b \end{aligned} \tag{2}$$

In Eq. (1), the values u_L, u_R, v_L, v_R are calculated as Eq. (3):

$$\begin{aligned} u_L &= [N_1\ N_2\ N_3\ N_4]\{u_1\ -\theta_1\ u_4\ -\theta_4\}^T \\ u_R &= [N_1\ N_2\ N_3\ N_4]\{u_2\ -\theta_2\ u_3\ -\theta_3\}^T \\ v_L &= [\bar{N}_1\ \bar{N}_2\ \bar{N}_3\ \bar{N}_4]\{v_1\ -\theta_1\ v_2\ -\theta_2\}^T \\ v_R &= [\bar{N}_1\ \bar{N}_2\ \bar{N}_3\ \bar{N}_4]\{v_4\ -\theta_4\ v_3\ -\theta_3\}^T \end{aligned} \tag{3}$$

in which $N_1\ N_2\ N_3\ N_4$ and $\bar{N}_1\ \bar{N}_2\ \bar{N}_3\ \bar{N}_4$ are cubic interpolation functions, and are defined as Eq. (4).

$$\begin{aligned} N_1 &= \frac{1}{2} - \frac{3s}{4} + \frac{s^3}{4} \\ N_2 &= \frac{1}{4} - \frac{s}{4} - \frac{s^2}{4} + \frac{s^3}{4} \\ N_3 &= \frac{1}{2} + \frac{3s}{4} - \frac{s^3}{4} \\ N_4 &= -\frac{1}{4} - \frac{s}{4} + \frac{s^2}{4} + \frac{s^3}{4} \\ \bar{N}_1 &= \frac{1}{2} - \frac{3r}{4} + \frac{r^3}{4} \\ \bar{N}_2 &= \frac{1}{4} - \frac{r}{4} - \frac{r^2}{4} + \frac{r^3}{4} \\ \bar{N}_3 &= \frac{1}{2} + \frac{3r}{4} - \frac{r^3}{4} \\ \bar{N}_4 &= -\frac{1}{4} - \frac{r}{4} + \frac{r^2}{4} + \frac{r^3}{4} \end{aligned} \tag{4}$$

Accordingly, the matrix of shape functions for FSE is obtained as Eq. (5):

$$\mathrm{N_{FS}}(r\ s) = \mathrm{M_N}(r\ s)\mathrm{T_r} \tag{5}$$

where, $\mathrm{M_N}$ is the matrix of the shape functions, and $\mathrm{T_r}$ is a transformation matrix of the relationship between the local rotations and the rotations at the nodes, defined in Eq. (6) and Eq. (7), respectively.
In $\mathrm{T_r}$, x_i and y_i are the coordinates of four-corner nodes. When the shape functions of the elements are obtained, the next step is the calculation of the strain–displacement (B) matrix. For the normalized (r, s) coordinate system this matrix is written as Eq. (8):

$$\mathrm{B} = \mathrm{A}\begin{bmatrix} \mathrm{J}^{-1} & 0 \\ 0 & \mathrm{J}^{-1} \end{bmatrix}\begin{bmatrix} \frac{\partial M_{N_1 i}}{\partial r} \\ \frac{\partial M_{N_1 i}}{\partial s} \\ \frac{\partial M_{N_2 i}}{\partial r} \\ \frac{\partial M_{N_2 i}}{\partial s} \end{bmatrix}\mathrm{T_r} \tag{6}$$

$$\mathrm{A} = \begin{bmatrix} 1 & 0 & 0 & 0 \\ 0 & 0 & 0 & 1 \\ 0 & 1 & 1 & 0 \end{bmatrix}$$

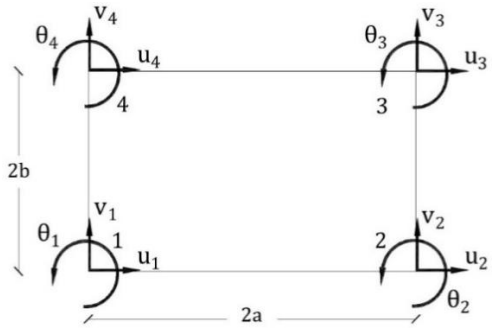

Fig. 1. A rectangular four-node element with drilling DOFs (θ_i).

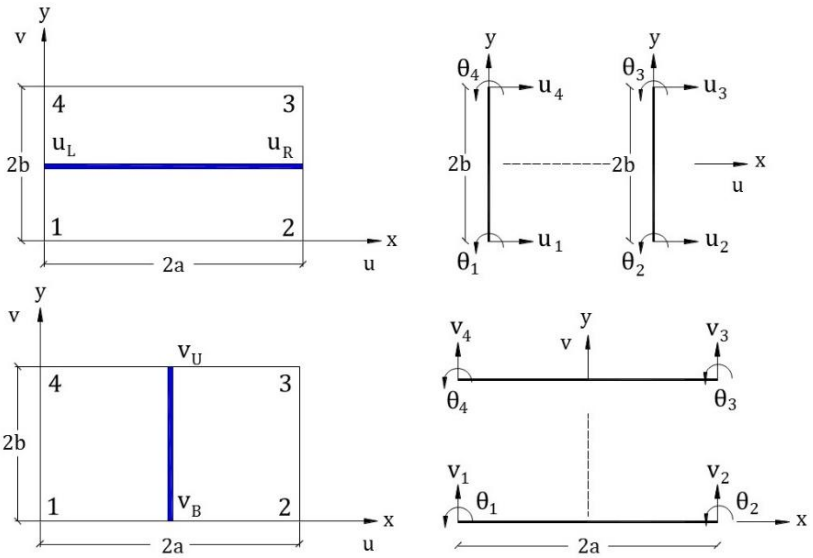

Fig. 2. The finite strips for a rectangular domain.

$$\mathbf{M_N}(r\ s) = \begin{bmatrix} M_1N_1 & 0 & -M_1N_2 & 0 & M_2N_1 & 0 & -M_2N_2 & 0 \\ 0 & \bar{M}_1\bar{N}_1 & 0 & \bar{M}_1\bar{N}_2 & 0 & \bar{M}_1\bar{N}_3 & 0 & \bar{M}_1\bar{N}_4 \\ M_2N_3 & 0 & -M_2N_4 & 0 & M_1N_3 & 0 & -M_1N_4 & 0 \\ 0 & \bar{M}_2\bar{N}_3 & 0 & \bar{M}_2\bar{N}_4 & 0 & \bar{M}_2\bar{N}_1 & 0 & \bar{M}_2\bar{N}_2 \end{bmatrix} \tag{7}$$

$$\mathbf{T_r} = \begin{bmatrix} 1 & 0 & 0 & 0 & 0 & 0 & 0 & 0 & 0 & 0 & 0 & 0 \\ 0 & 1 & 0 & 0 & 0 & 0 & 0 & 0 & 0 & 0 & 0 & 0 \\ 0 & 0 & (y_4-y_1)/2 & 0 & 0 & 0 & 0 & 0 & 0 & 0 & 0 & 0 \\ 0 & 0 & (x_2-x_1)/2 & 0 & 0 & 0 & 0 & 0 & 0 & 0 & 0 & 0 \\ 0 & 0 & 0 & 1 & 0 & 0 & 0 & 0 & 0 & 0 & 0 & 0 \\ 0 & 0 & 0 & 0 & 1 & 0 & 0 & 0 & 0 & 0 & 0 & 0 \\ 0 & 0 & 0 & 0 & 0 & (y_3-y_2)/2 & 0 & 0 & 0 & 0 & 0 & 0 \\ 0 & 0 & 0 & 0 & 0 & (x_2-x_1)/2 & 0 & 0 & 0 & 0 & 0 & 0 \\ 0 & 0 & 0 & 0 & 0 & 0 & 1 & 0 & 0 & 0 & 0 & 0 \\ 0 & 0 & 0 & 0 & 0 & 0 & 0 & 1 & 0 & 0 & 0 & 0 \\ 0 & 0 & 0 & 0 & 0 & 0 & 0 & 0 & (y_3-y_2)/2 & 0 & 0 & 0 \\ 0 & 0 & 0 & 0 & 0 & 0 & 0 & 0 & (x_3-x_4)/2 & 0 & 0 & 0 \\ 0 & 0 & 0 & 0 & 0 & 0 & 0 & 0 & 0 & 1 & 0 & 0 \\ 0 & 0 & 0 & 0 & 0 & 0 & 0 & 0 & 0 & 0 & 1 & 0 \\ 0 & 0 & 0 & 0 & 0 & 0 & 0 & 0 & 0 & 0 & 0 & (y_4-y_1)/2 \\ 0 & 0 & 0 & 0 & 0 & 0 & 0 & 0 & 0 & 0 & 0 & (x_3-x_4)/2 \end{bmatrix} \tag{8}$$

where J is the Jacobian matrix and could be written as Eq. (9).

$$\mathbf{J} = \begin{bmatrix} \frac{\partial X(r\,s)}{\partial r} & \frac{\partial Y(r\,s)}{\partial r} \\ \frac{\partial X(r\,s)}{\partial s} & \frac{\partial Y(r\,s)}{\partial s} \end{bmatrix}$$
$$\mathbf{J}^{-1} = \frac{1}{|\mathbf{J}|}\begin{bmatrix} \frac{\partial Y(r\,s)}{\partial s} & \frac{-\partial Y(r\,s)}{\partial r} \\ \frac{-\partial X(r\,s)}{\partial s} & \frac{\partial X(r\,s)}{\partial r} \end{bmatrix} \tag{9}$$

The relation between normalized and global coordinates system is presented as Eq. (10).

$$\begin{aligned} X(r,s) &= \textstyle\sum_{i=1}^{4} N_i(r,s)x_i \\ Y(r,s) &= \textstyle\sum_{i=1}^{4} N_i(r,s)y_i \end{aligned} \tag{10}$$

In this method, the geometry of the strip element is described in a normalized coordinate system, and the bilinear shape functions are explained as Eq. (11).

$$N_i(r\ s) = \frac{1}{4}(1 + r_i r)(1 + s_i s)$$
$$r_i = [-1 \quad 1 \quad 1 \quad -1]$$
$$s_i = [-1 \quad -1 \quad 1 \quad 1] \qquad (11)$$

For $i = 1\ to\ 4$.

2.2. Stiffness and mass matrices and Nodal forces

After obtaining the shape functions and strain matrixes, the calculations of stiffness and mass matrices are available [24]. First, the stiffness matrix is computed as Eq. (12):

$$\mathbf{K_e} = t \iint \mathbf{B}^T\mathbf{D}\mathbf{B}dA = t \int_{-1}^{1}\int \mathbf{B}^T\mathbf{D}\mathbf{B}|\mathbf{J}|drds \qquad (12)$$

in which, t defines the thickness of the element; B indicates the strain matrix, D refers to the material matrix, and $|\mathrm{J}|$ is the determinant of the Jacobian matrix. For plane stress or strain type problems, the material matrixes are written as Eq. (13):

$$\mathbf{D} = \frac{E}{1-\nu^2}\begin{bmatrix} 1 & \nu & 0 \\ \nu & 1 & 0 \\ 0 & 0 & \frac{1-\nu}{2} \end{bmatrix}$$

For plane-stress problems,

$$\mathbf{D} = \frac{E(1-\nu)}{(1+\nu)(1-2\nu)}\begin{bmatrix} 1 & \frac{\nu}{1-\vartheta} & 0 \\ \frac{\nu}{1-\nu} & 1 & 0 \\ 0 & 0 & \frac{1-2\nu}{2(1-\nu)} \end{bmatrix} \qquad (13)$$

For plane-strain problems

where E and ν are Yong modulus and Poisson ratio of the materials, respectively. Eq. (14) is used to obtain the mass matrix:

$$\mathbf{M_e} = \rho t \iint \mathbf{N_{FS}^T}\mathbf{N_{FS}}dA = t \int_{-1}^{1}\int \mathbf{N_{FS}^T}\mathbf{N_{FS}}|\mathbf{J}|drds \qquad (14)$$

where ρ is the mass density. It should be noted that the obtained mass matrix, according to Eq. (14), is not diagonal. For reducing the computational costs in dynamic analyses, and appropriate performance in frequencies calculations, the mass matrix should be diagonalized. This process is conducted according to the following steps [24, 25]:

1. Compute only diagonal coefficients m_{ii} of the consistent element mass matrix.
2. For each coordinate direction in which the element DOFs describe motion, two sub-steps should be followed:
   2a. Determine a number s by adding the m_{ii} associated with translational DOF (not rotational DOFs).
   2b. Multiply all coefficients m_{ii} associated with this direction by the ratio m/s.

The diagonal mass matrix is used for the calculation of Eigen-values to obtain the Rayleigh damping matrix. When the mass and stiffness matrices are obtained, the assembled matrixes are produced, and the Rayleigh damping matrix could be explained as Eq. (15) [26, 27]:

$$\mathbf{C} = \left(2\xi\frac{\omega_1\omega_j}{\omega_1+\omega_j}\right)\mathbf{M} + \left(\frac{2\xi}{\omega_1+\omega_j}\right)\mathbf{K} \qquad (15)$$

where, ω_1 and ω_j refer to the first and last available natural frequencies of the system, respectively. Besides, ξ is the damping ratio and is set to 0.05. The equivalent nodal forces for each element could be written as Eq. (16).

$$\mathbf{f_e} = t \int_{-1}^{1}\int \mathbf{N_{FS}^T}\mathbf{b}|\mathbf{J}|drds + t \int_{-1}^{1} \mathbf{N_{FS}^T}\mathbf{q_e}ds \qquad (16)$$

Here, $\mathrm{q_e}$ is the equivalent nodal force due to body and surface traction loadings. The $\mathrm{b}_{2\times1}$ is the gravity or body force vector and $(\mathrm{q_e})_{2\times1}$ refers to the intensity of surface traction load along any side of the element.

3. Time history analysis using FSE

After the calculation of mass, damping, and stiffness matrices, the equation of motion for a structural system in the time domain is written as Eq. (17).

$$\mathrm{M\ddot{u} + C\dot{u} + Ku = P_{eff} = -Mr\ddot{u}_g} \qquad (17)$$

Here, r is the influence vector to insert the direction of earthquake record, and $\ddot{u}_g$ is the ground acceleration. For solving the equilibrium equation in time history loadings, the linear acceleration Newmark algorithm is used [28]. The main steps for the calculation of time history responses are presented in Fig. 3. The described formulations in Sections 2, 3 are programmed in the MATLAB environment.

4. Numerical studies

For validating of the proposed formulation, according to Fig. 4, three plane-stress problems are studied. The cases are named Fig. 4(a) models (I), Fig. 4 (b) model (II), and Fig. 4 (c) model (III). Model (I), is a Bernoulli-type beam. The second model (II) could be considered as a Bernoulli or a Timoshenko beam. Finally, the third model (III) is a Timoshenko beam. For comparing the results of each model, three finite-element models, in different mesh sizes, are proposed. The numerical results of the static responses and natural frequencies are compared with the analytical results.

Material properties for static and dynamic analyses of the mentioned models have been presented in Table 1.

4.1. Validations and results

4.1.1. Displacements and rotations

The responses of the mentioned models are compared using analytical, numerical (commercial finite-element software), and the presented method.

Firstly, a concentrated load *P* at node A is applied for the static responses of each model. Then, the static displacements of all DOF's are computed using the proposed formulations.

The analytical displacement at A and stress at B are calculated using the Bernoulli beam theory for model (I) as Eq. (18):

$$\Delta_A = \frac{Pl^3}{3EI} \quad , \sigma_B = \frac{M}{S} = \frac{Pl}{I/C} = \frac{6Pl}{th^2} \tag{18}$$

Table 1. Material properties of the case studies.

Modulus of elasticity	Mass density	Poisson ratio	P(kN)
21 GPa	2400 kg/m^3	0.25	100

Initialization of the variables

1. Initial conditions at $t = 0$: $\mathbf{u}_0$, $\dot{\mathbf{u}}_0$; determination of $\ddot{\mathbf{u}}_0$:

$$\mathbf{M}\ddot{\mathbf{u}}_0 = \mathbf{p}_0 - \mathbf{C}\dot{\mathbf{u}}_0 - \mathbf{K}\mathbf{u}_0.$$

2. Selection of integration time step Δt, $\Delta t \leq \Delta t_{\text{cr}} = T_{n_{eq}}/\pi$.

Preliminary calculations

1. Calculation of integration constants

$$a_0 = \frac{1}{\Delta t^2}; \quad a_1 = \frac{1}{2\Delta t}; \quad a_2 = \frac{2}{\Delta t^2}; \quad a_3 = \frac{\Delta t^2}{2}.$$

2. Calculation of displacement vector $\mathbf{u}_{-1}$: $\mathbf{u}_{-1} = \mathbf{u}_0 - \Delta t\dot{\mathbf{u}}_0 + a_3\ddot{\mathbf{u}}_0$.
3. Calculation of effective stiffness matrix $\hat{\mathbf{K}}$: $\hat{\mathbf{K}} = a_0\mathbf{M} + a_1\mathbf{C}$.
4. Factorization of $\hat{\mathbf{K}}$: $\hat{\mathbf{K}} = \mathbf{L}\mathbf{D}\mathbf{L}^{\mathsf{T}}$.

Step-by-step integration: for $n = 0, 1, 2, \ldots, t_d/\Delta t$

1. Increment time: $t_{n+1} = t_n + \Delta t = (n+1)\Delta t$, $t_0 = 0$.
2. Calculation of effective forces vector $\hat{\mathbf{p}}_n$ at time t_n:

$$\hat{\mathbf{p}}_n = \mathbf{p}_n - (a_0\mathbf{M} - a_1\mathbf{C})\,\mathbf{u}_{n-1} - (\mathbf{K} - a_2\mathbf{M})\,\mathbf{u}_n.$$

3. Calculation of displacement vector at time t_{n+1}:

$$\mathbf{L}\mathbf{D}\mathbf{L}^{\mathsf{T}}\mathbf{u}_{n+1} = \hat{\mathbf{p}}_n.$$

4. Calculation of acceleration and velocity vectors at time t_n, if required:

$$\ddot{\mathbf{u}}_n = a_0\,(\mathbf{u}_{n-1} - 2\mathbf{u}_n + \mathbf{u}_{n+1}),$$

$$\dot{\mathbf{u}}_n = a_1\,(\mathbf{u}_{n+1} - \mathbf{u}_{n-1}).$$

Fig. 3. Steps of numerical integration using Newmark methods for MDOF systems.

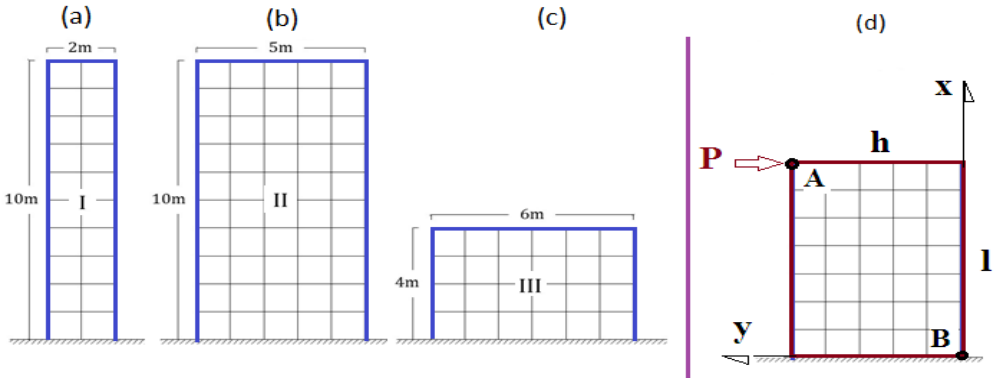

Fig. 4. Studied models; (a) model I, (b) model II, (c) model III and (d) general model.

Table 2. Deformation responses of the model (I) at point A.

Mesh size	Method	Displacements		
		$\Delta_x(mm)$	$\Delta_y(mm)$	$\theta\ (rad)$
10×2	Finite strip	**0.393**	**2.60**	7.31×10^{-4}
	ABAQUS	0.500	3.30	$3.30\times10^{-4*}$
20×4	Finite strip	**0.386**	**2.50**	8.39×10^{-4}
	ABAQUS	0.400	2.70	$2.70\times10^{-4*}$
30×6	Finite strip	**0.387**	**2.50**	9.62×10^{-4}
	ABAQUS	0.400	2.60	$2.60\times10^{-4*}$
No mesh	Timoshenko	-	2.50	-
	Bernoulli	0.736	2.40	3.57×10^{-4}

* The values have been calculated by hand, and the software could not predict the rotations.

where P is a concentrated load, E is the modulus of elasticity, l is the length and h is the height of the studied models. I refers to the moment of inertia and t refers to the thickness of the model. In the Timoshenko beam theory, the displacements and rotations at any point could be calculated as Eq. (19).

$$\begin{aligned}
&\Delta_A = \frac{Pl^3}{3EI} \quad , \quad \sigma_B = \frac{M}{S} = \frac{Pl}{I/C} = \frac{6Pl}{th^2} \\
&\Delta_x = \frac{P}{EI}\left[\frac{\nu(l-x)}{2}y^2 + \frac{lx^2}{2} - \frac{x^3}{6} + \frac{(1+\nu)h^2x}{4}\right] \\
&\Delta_y = \frac{P}{6EI}[3xy(2l-x) + (2+\nu)y^3] \\
&\theta_z = \frac{P}{2EI}\left[2lx - x^2 + y^2 + \frac{(1+\nu)h^2}{4}\right]
\end{aligned} \tag{19}$$

Besides, for the validation of the proposed formulation for dynamic analysis, the first three frequencies of Bernoulli type beams have been analytically calculated as Eq. (20).

$$\omega_1 = \frac{3{,}516}{l^2}\sqrt{\frac{EI}{m}} \tag{20}$$

$$\omega_2 = \frac{22{,}03}{l^2}\sqrt{\frac{EI}{m}}$$

$$\omega_3 = \frac{61{,}7}{l^2}\sqrt{\frac{EI}{m}}$$

Here, m refers to the mass per unit length of the studied models. When analytical solutions are not available for finding the responses, the commercial ABAQUS software [29] has been applied. For modeling such problems, the CPS4R element is used from the element library of the software. This element comprises eight translational DOFs.

In Table 2 the displacements and the rotations of model I are presented. This model could be considered as a Bernoulli beam model, and for comparing the results of this beam, three mesh sizes are studied.

As seen in Table 2, when the number of elements is changed, the obtained values from ABAQUS have more variations. Moreover, the variations of FSE's results are negligible when the mesh sizes are changed.

Table 3. Deformation responses of the model (II) at point A.

Mesh size	Method	Displacements		
		$\Delta_x\ (mm)$	$\Delta_y\ (mm)$	$\theta\ (rad)$
10×5	Finite strip	**0.085**	**0.210**	1.60×10^{-4}
	ABAQUS	0.097	0.230	$2.30\times10^{-5*}$
20×10	Finite strip	**0.089**	**0.220**	2.80×10^{-4}
	ABAQUS	0.093	0.240	$2.40\times10^{-5*}$
30×15	Finite strip	**0.092**	**0.230**	4.10×10^{-4}
	ABAQUS	0.093	0.240	$2.40\times10^{-5*}$
No mesh	Timoshenko	0.140	0.190	3.00×10^{-5}
	Bernoulli	-	0.150*	$2.29\times10^{-5*}$

* The values have been indirectly calculated by hand, and the software could not predict the rotations

Table 4. Responses of the model (III) at point A.

Mesh size	Method	Displacements		
		$\Delta_x\ (mm)$	$\Delta_y\ (mm)$	$\theta\ (rad)$
10×5	Finite strip	$\mathbf{5.24\times10^{-2}}$	$\mathbf{3.51\times10^{-2}}$	1.2×10^{-4}
	ABAQUS	5.32×10^{-2}	3.09×10^{-2}	$1.3\times10^{-5*}$
20×10	Finite strip	$\mathbf{5.92\times10^{-2}}$	$\mathbf{4.02\times10^{-2}}$	2.5×10^{-4}
	ABAQUS	6.61×10^{-2}	3.78×10^{-2}	$1.7\times10^{-5*}$
30×15	Finite strip	$\mathbf{6.32\times10^{-2}}$	$\mathbf{4.19\times10^{-2}}$	3.8×10^{-4}
	ABAQUS	7.34×10^{-2}	4.21×10^{-2}	$1.8\times10^{-5*}$
No mesh	Timoshenko (Exact)	1.83×10^{-2}	3.43×10^{-2}	8.4×10^{-6}

* The values have been calculated by hand, and the software could not predict the rotations

Therefore, the present method has good performance for the prediction of displacements even for coarse meshes. This advantage is valuable in dynamic and nonlinear analyses because the computational costs for coarse meshes are less than fine meshes. Besides, the results of Table 2 show that variations of rotations from FSE are significant and even by reducing the mesh sizes, the errors are increased. In ABAQUS, the rotations for the nodes were not available, and they were calculated by hand.

In Table 3, the deformation responses of the model (II) are presented. This model could be considered as a Bernoulli or Timoshenko beam model. Therefore, analytical solutions for this model are available. As seen from Table 3, in comparison with the exact values, the proposed method using even coarse mesh (2×10) has acceptable displacement results. By increasing the mesh sizes, the numerical results were not improved. For rotations, similar to the model (I), the errors of FSE are significant in comparison with the exact values. It should be noted that the rotations obtained by ABAQUS are based on hand calculations.

Model (III) is a Timoshenko-type beam, and an analytical solution for this model is available as Eq. (19). As seen in Table 4, the proposed method with coarse mesh (5×10) has reasonable performance. In all mesh sizes, FSE formulation presents better results in comparison with the commercial finite-element software. Similar to models (I), (II), the errors of the rotations are notable.

The rotational results show that in all models, in comparison with analytical results, the values of the finite strip method are significant. Therefore, the proposed FSE formulation presents softer values than the responses of finite element software. Moreover, in all models, the displacements are more accurate than the rotational values.

4.1.2. Stresses and frequencies

In the finite-strip element, the stresses at any point are obtained as Eq. (21):

$$\sigma = D\varepsilon \tag{21}$$

where D and ε are the material matrix and strain vector, respectively. The stresses in Bernoulli and Timoshenko beams could be obtained according to Eq. (21). The results of stresses using analytical, numerical, and finite strip methods are presented in Fig. 5. The results show that in Fig. 5. (b) model (II) and in Fig. 5. (c) model (III) approximately have similar

results; and mesh sizes have no significant effects on the variations of stresses. Moreover, in model (I), for all mesh sizes, the FSE method presents a better performance in comparison with ABAQUS Software.

Fig. 6 presents the results of the first three frequencies of the studied models. In model (I), the errors of the first frequency are negligible. However, the error of the second frequency obtained from ABAQUS for coarse mesh is large. The second frequency (ω_2) calculated from FSE is not sensitive to mesh size. Moreover, this frequency calculated by ABAQUS is sensitive to the mesh size. For ω_3, the results of FSE and the exact method are the same, and mesh sizes have no significant effects on the variations of the frequencies. Even though the ABAQUS results are more sensitive to the changing of mesh sizes, the errors are notable.

The second and third graphs of Fig. 6 illustrate the results of the first three frequencies for Fig. 6(b) model (II) and Fig. 6(c) model (III). Here, the error of the first frequency is small. The second frequency (ω_2) calculated by FSE is not sensitive to the mesh dimensions. However, this frequency obtained by ABAQUS is very sensitive to the number of elements. For ω_3 the results of FSE and analytical /exact methods are the same. Even so, the results of ABAQUS software are sensitive to the mesh dimensions.

Briefly, the errors of the first frequencies in all models are negligible against mesh sizes; however, in all models, the second and third frequencies (ω_2, ω_3) using FSE formulations are not sensitive to the mesh size. The frequencies obtained by ABAQUS are sensitive to the mesh size.

4.1.3. Dynamic responses

For calculating the dynamic responses of the described models, three strong ground motions are considered. The horizontal components of El-Centro, Kobe, and Tabas earthquakes were selected from the PEER database [30]. The acceleration time histories of the mentioned records are shown in Fig. 7.

Fig. 8 presents the results of the dynamic responses of the model (I) against the Tabas earthquake. As seen from this figure, FSEFSE results are not sensitive to the change of elements number. Moreover, the results of finite-element modeling, ABAQUS, are very sensitive to the mesh dimensions. Therefore, to get reliable values of responses using finite-element modeling, the trial–error procedure should be performed for finding the proper mesh size. Unlike the finite-element model, the FSE produces acceptable results for any mesh size. This preference is vital in the numerical modeling of structures in dynamic analysis and nonlinear cases.

Table 5 shows the maximum horizontal displacements of model (I) against various mesh sizes against the Tabas record. The results show a small difference, 2 mm, when using coarse meshes, 2×10, and fine meshes, 6×30. Moreover, in the finite-element method, the difference between coarse mesh, 2×10, and fine mesh, 6×30 is 11 mm. Therefore, applying the proposed FSE method is not sensitive to the mesh sizes, and is interested in the numerical analyses.

To parametric study, Fig. 9 presents the dynamic responses of a FSE method for studied models against Tabas, El-Centro, and Kobe records. As seen from this figure, the peak values of the horizontal displacements belong to El-Centro records. The responses of Fig. 9 are obtained from coarse mesh sizes (2×10).

Table 6 shows the maximum horizontal displacements of models against triple records for coarse meshes. The mentioned values in Table 5 are approximately obtained from Fig. 9.

Table 5. Maximum displacements of the model (I) at point A v.s. mesh sizes.

Mesh size	Δ_x(max) (mm)	
	FSE	ABAQUS
2×10	27	41
4×20	25	38
6×30	25	29

Table 6. Maximum displacements of models against the records.

Record	Δ_x(max) (mm)		
	Model (I)	Model (II)	Model (III)
Tabas	25.0	4.0	0.2
El-Centro	46.0	8.0	0.4
Kobe	14.0	3.0	0.1

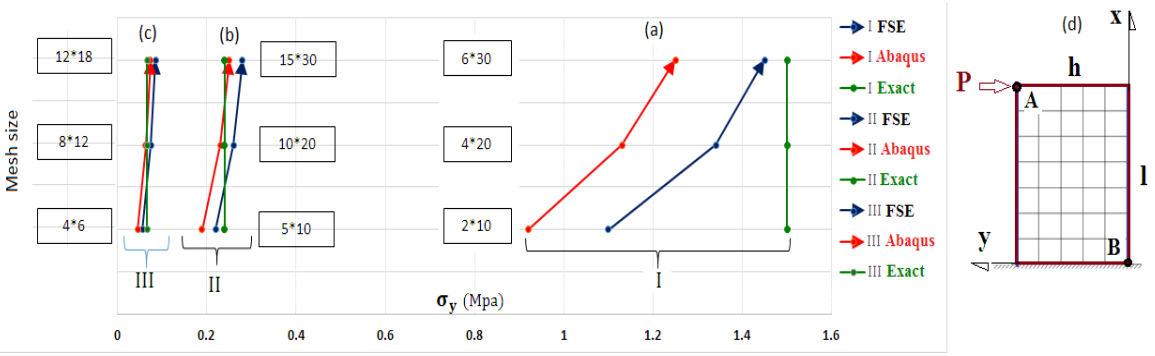

Fig. 5. Stress response of studied models (values are at point B); (a) model I, (b) model II, (c) model III and (d) general model.

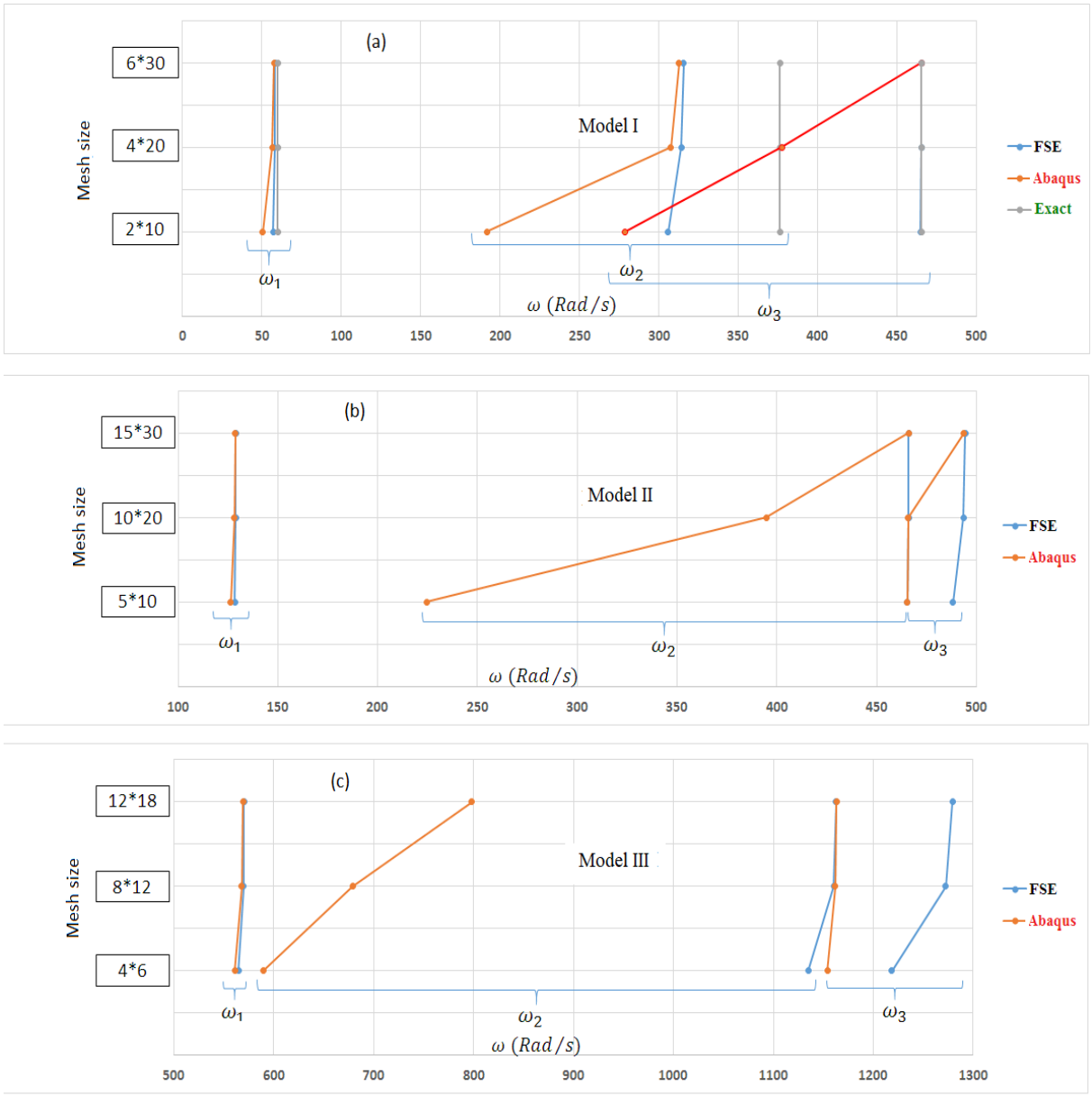

Fig. 6. Comparison of calculated frequencies for studied models; (a) model I, (b) model II and (c) model III.

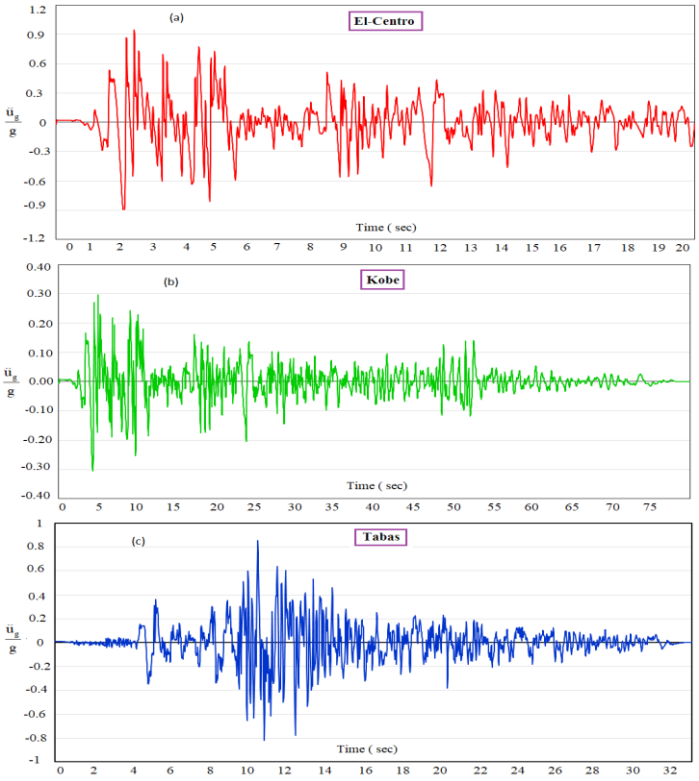

Fig. 7. Acceleration time histories of the horizontal component; (a) El-Centro record, (b) Kobe record and (c) Tabas record.

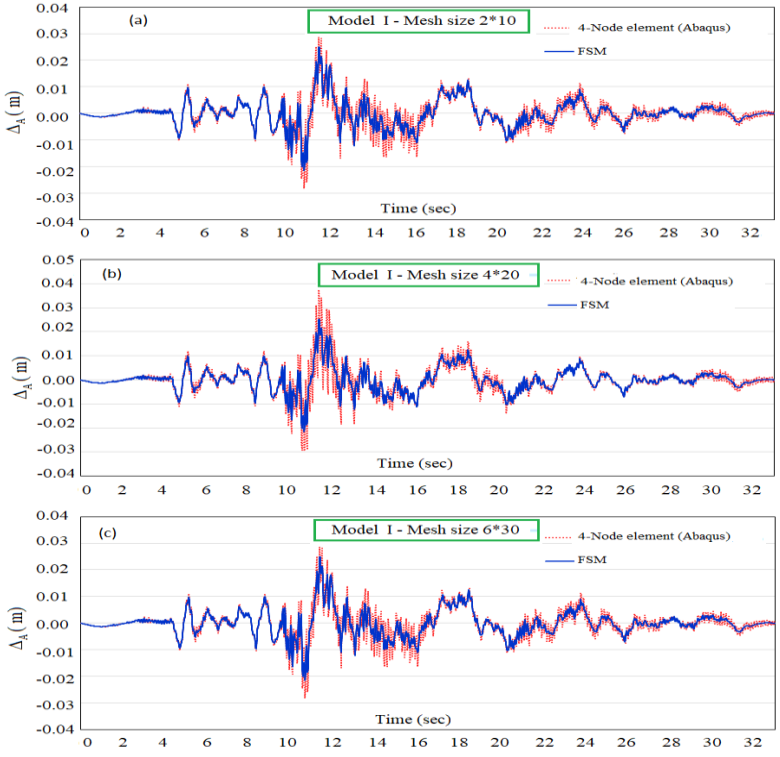

Fig. 8. Dynamic responses of Model I against Tabas earthquake v.s mesh dimensions; (a) mesh size 2x10, (b) mesh size 4x20 and (c) mesh size 6x30.

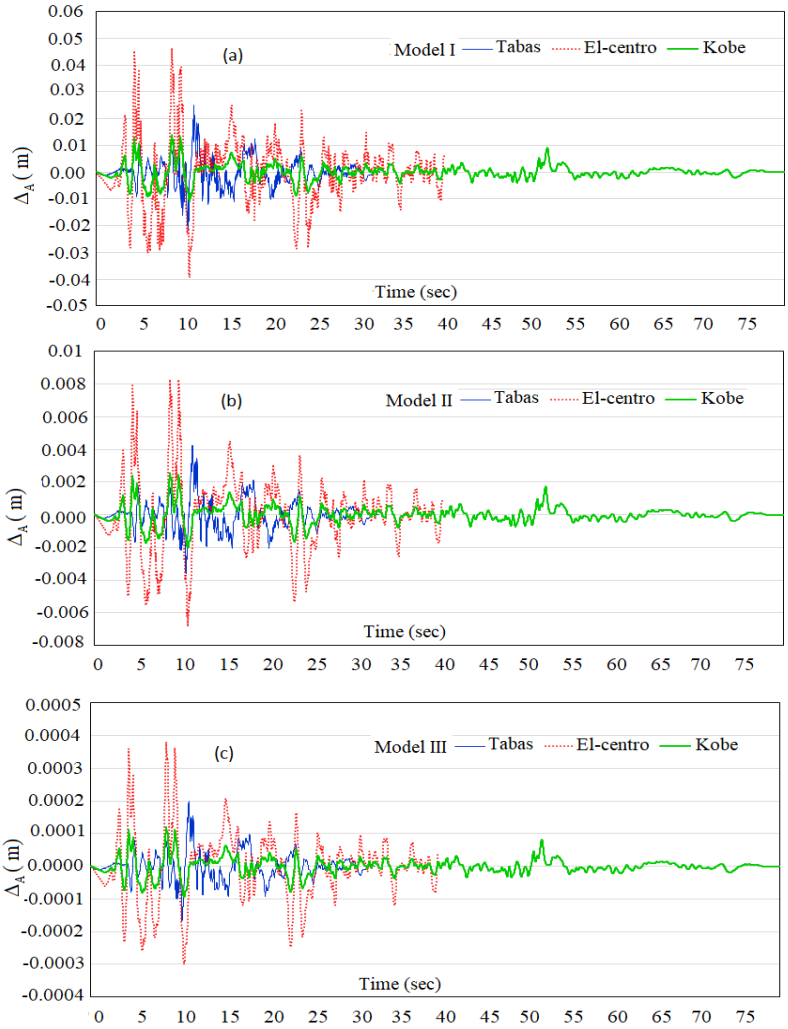

Fig. 9. Dynamic responses of studied models against Tabas, El-Centro, and Kobe records; (a) model I, (b) model II and (c) model III.

5. Conclusions

This paper presents the finite strip method for dynamic analyses of plane stress and strain problems, including drilling DOF. For this purpose, a computer program in the MATLAB environment is provided and validated. Based on the present study, the following conclusions are drawn:

1. The proposed element has twelve degrees of freedom and is softer than four-node rectangular elements, including eight degrees of freedom.
2. In all studied models, the present formulation has good performance for the prediction of displacements, even when coarse meshes are used. This advantage is valuable in dynamic and nonlinear analyses because the computational costs using coarse meshes are preferable.
3. The rotational results show that in all studied models, the values of the finite strip method are more than analytical results. Therefore, the proposed FSE formulation presents softer values than the responses of the finite-element method. Moreover, in all models, the displacements are more accurate than the rotational values.
4. The errors of first frequencies in all models are negligible against mesh sizes. Additionally, in all models, the values of higher frequencies using present formulations are not sensitive to the mesh

size. However, the frequencies obtained from the finite-element method are very sensitive to the mesh sizes.

5. The dynamic responses show small differences between using coarse meshes and fine meshes. Moreover, in the finite-element method, the differences or responses between coarse meshes and fine meshes are large. Therefore, applying the proposed FSE method is not sensitive to mesh sizes, and is preferable in numerical analyses.
6. The most significant advantage of this formulation is that using coarse meshes is sufficient to obtain reliable results, and the computational time in large-scale problems is cost-effective.

Acknowledgments

The first author acknowledged the support from Malayer University when he was an assistant professor of Civil Engineering before June 2019.

Competing interests

The authors declare that they have no competing interests.

References

[1] R. H.Wang, "A rectangular plate bending element based upon finite strip in length and breadth", *J. Eng. Mech*., Vol. 17, No. 1, pp. 114-119, (2000).

[2] M. H. Huang and D. P. Thambiratnam, "Analysis of plate resting on elastic supports and elastic foundation by finite strip method ", *Comput. Struct*., Vol. 79, No. 30,pp. 2547-2557, (2001).

[3] G. R. Liu," A combined finite element/strip element method for analyzing elastic wave scattering by cracks and inclusions in laminates", *Comput. Mech.*, Vol. 28, No. 1, pp. 76-82, (2002).

[4] H. M. Liu, P. Yan, C. Yu-Peng and W. Ying-Rui, "Strip element method for shape discrimination of strip rolling", *Commun. Numer. Methods Eng.*, Vol. 20, No. 9, pp. 709-720, (2004).

[5] G. Xia, M. Yu, C. Li and J. Zhang, "Rectangular Membrane Element with Rotational Degree of Freedom", *J. Comput. Struct. Eng.*, Vol. 23, No. 2, pp. 1051-1058, (2009).

[6] F. Rojas, J. C. Anderson and L. M. Massone, "A nonlinear quadrilateral layered membrane element with drilling degrees of freedom for the modeling of reinforced concrete walls", *Eng. Struct.*, Vol. 12, No. 4, pp. 521-538, (2016).

[7] F. Wang, J. Zhang and L .Jiang, "Analysis of Single Cell Curved Box Girder Bases on Finite Strip Element Theory", *In 2017 5th International Conference on Mechatronics, Materials, Chemistry and Computer Engineering, ICMMCCE*, (2017).

[8] B. W.Schafer, "Elastic buckling analysis of thin-walled members using the classical finite strip method", *CUFSM* Version, 2, (2003).

[9] B. W. Schafer and S. Adany, "Buckling analysis of cold-formed steel members using CUFSM: conventional and constrained finite strip methods", *In Eighteenth international specialty conference on cold-formed steel structures*, pp. 39-54, (2006).

[10] G. Eccher, K. J. R. Rasmussen and R. Zandonini, " Linear elastic isoperimetric spline finite strip analysis of perforated thin-walled structures", *Thin-Walled Struct.*, Vol. 46, No. 3, pp. 242-260 (2008).

[11] S. A. M. Ghannadpour, H. R. Ovesy and M. Nassirnia, "Buckling analysis of functionally graded plates under thermal loadings using the finite strip method", *Comput Struct*, Vol. 108, No. 1, pp. 93-99, (2012).

[12] L. K. Yao, B. He, Y. Zhang and W. Zhou, "Semi-analytical finite strip transfer matrix method for buckling analysis of rectangular thin plates", *Math. Probl. Eng.* Vol. 23, No. 1, pp. 230-241,(2015).

[13] Q. Chen and P. Qiao, "Buckling analysis of laminated plate structures with elastic

edges using a novel semi-analytical finite strip method", *Compos. Struct.*, Vol. 152, No. 1, pp. 85-95, (2016).

[14] B. He, Y. Zhang, W. Y. Ge, Y. An and D. Liu, "Buckling analysis of thin-walled members with open-branched cross-section via semi-analytical finite strip transfer matrix method", *Thin-Walled Struct.*, Vol. 124, No. 1, pp. 20-31, (2018).

[15] Z. Li and B. W. Schafer, "Application of the finite strip method in cold-formed steel member design", *J. Constr. Steel Res.*, Vol. 66, No. 8, pp. 971-980 (2010).

[16] L. Zhen, P. Qiao, J. Zhong, Q. Chen, J. J. Chen and J. H.Wang, "Design of steel pipe-jacking based on buckling analysis by finite strip method", *Eng. Struct*., Vol. 132, No. 1, pp. 139-151, (2017).

[17] S. S. Ajeesh and S. A. Jayachandran, "A constrained spline finite strip method for the mode decomposition of cold-formed steel sections using GBT principles", *Thin-Walled Struct.*, Vol. 113, No. 1, pp. 83-93, (2017).

[18] Q. Chen and P. Qiao, "Post-buckling analysis of composite plates under combined compression and shear loading using the finite strip method", *Finite Elem. Anal. Des.*, Vol. 83, No. 1, pp. 33-42, (2014).

[19] S. Wang and Y. Zhang, "Vibration analysis of rectangular composite laminated plates using a layerwise B-spline finite strip method", *Compos. Struct.*, Vol. 68, No. 3, pp. 349-358 (2005).

[20] R. J. Jiang and F. T. K. Au, "A general finite strip for the static and dynamic analyses of folded plates", *Thin-Walled* Struct., Vol. 49, No. 10, pp. 1288-1294, (2011).

[21] J. Poblet-Puig and A. Rodriguez-Ferran, "The finite strip method for acoustic and vibroacoustic problems", *J. Comput. Acoust.*, Vol. 19, No. 4, pp. 353-378, (2011).

[22] I. Senjanović, I. Áatipović, N. Alujević, D. Čakmak and N. Vladimir, "A finite strip for the vibration analysis of rotating toroidal shell under internal pressure", *J. Vib. Acoust.*, Vol. 141, No. 2, 021013, (2019).

[23] MATLAB, *The MathWorks*, Inc., Natick, (2018).

[24] R. D.Cook, *"Concepts and applications of finite element analysis"*, John Wiley & sons (2007).

[25] V. Shánel, R. Kolman and J. Plešek, "Mass Lumping methods for the Semi-Loof Shell Elements", *J. Eng. Mech.*, Vol. 122, No.1, pp. 1161-1171, (2012).

[26] A. K. Chopra, "*Dynamics of Structures Theory and Applications to Earthquake Engineering", 4th*. Prentice-Hall: Englewood Cliffs, NJ, (2012).

[27] A. S. Elnashai and L. Di Sarno," *Fundamentals of earthquake engineering* ", New York: Wiley, (2008).

[28] P. Paultre, *"Dynamics of structures*", John Wiley & Sons, (2013).

[29] ABAQUS, "*Standard user's manual*", Hibbitt, Karlsson and Sorenson, Inc, (2014).

[30] PEER *Strong Motion Database. Pacific Earthquake Engineering Research Center* University of California, Berkeley. Available Online at http://peer.berkeley.edu, (2015).

How to cite this paper:

J. Akbari, H. Valaei and M. F. Sepahvand, " Numerical response using finite strip element including drilling degree of freedom,", *J. Comput. Appl. Res. Mech. Eng.*, Vol. 12, No. 2, pp. 177-191, (2023).

DOI: 10.22061/JCARME.2022.6916.1894

URL: https://jcarme.sru.ac.ir/?_action=showPDF&article=1715